

BMP-7 Modulates Hyaluronan-Mediated Proximal Tubular Cell-Monocyte Interaction

WISAM SELBI,* CAROL DE LA MOTTE,[†] VINCENT HASCALL,[†] and ALED PHILLIPS*

**Institute of Nephrology, University of Wales College of Medicine, Heath Park, Cardiff, Wales, United Kingdom; and* [†]*Department of Biomedical Engineering, The Cleveland Clinic Foundation, Cleveland, Ohio.*

Abstract. Increased synthesis of hyaluronan (HA) in the renal corticointerstitium has been documented in renal injury, although the functional significance of this is unclear. The aim of the work presented in the current study was to examine the role of HA in monocyte binding by proximal tubular cells (PTC). Using the PTC line HK-2, the authors show that unstimulated cells formed pericellular HA cable-like structures that bound mononuclear leukocytes via their cell surface CD44. Stimulation with bone morphogenic protein-7 (BMP-7) led to increased formation of HA cable-like structures and also a dose-dependent increase in CD44-dependent binding of radiolabeled U937 cells. The authors have previously demonstrated that stimulation with IL-1 β is a potent stimulus for induction of HAS gene expression and HA synthesis. In this study, addition

of IL-1 β influenced neither HA cable formation nor CD44-mediated monocyte binding. Rather IL-1 β led to an increase in intercellular adhesion molecule (ICAM)-dependent monocyte binding. Characterization of HA synthesis by addition of [³H]-glucosamine to cells at the time of stimulation demonstrated that increased HA in response to IL-1 was most apparent in the culture medium, while BMP-7 led to an increase in cell associated HA. Stimulation of cells with BMP-7 induced HAS2 mRNA expression and decreased the expression of Hyal1 and Hyal2. In contrast to BMP-7, IL-1 β did not influence Hyal expression. The data presented in this manuscript provide insight into how alterations in HA synthesis in the renal cortex may be involved in modulation of the interaction between infiltrating inflammatory cells and resident cells.

Hyaluronan (HA) is a ubiquitous connective tissue glycosaminoglycan that *in vivo* is present as a high-molecular mass component of the extracellular matrix. In addition to its role in providing cellular support, it is now known that under normal circumstances, HA regulates cell-cell adhesion, migration, proliferation, differentiation, and the movement of interstitial fluid and macromolecules (reviewed in reference 1). As a result, it is likely to be an important contributor to and a regulator of wound healing and tissue remodeling.

In the normal kidney, HA is expressed in the interstitium of the renal papilla only, and alteration in papillary interstitial HA has been implicated in regulating renal water handling by affecting physicochemical characteristics of the papillary interstitial matrix and influencing the interstitial hydrostatic pressure (2). More recently, alterations in HA synthesis within the glomerulus of the kidney have been implicated in the pathogenesis of renal diseases such as diabetic nephropathy (3,4). Although HA is not a major constituent of the normal renal corticointerstitium, it is known to be expressed around proximal tubular cells (PTC)

after renal injury caused by diverse diseases (5–8). Furthermore, increased deposition of interstitial HA has been shown to correlate with both proteinuria and renal function in progressive renal disease (9).

With the increasing awareness of the importance of pathologic changes in the renal interstitium, interest has focused on the role of cells, such as the epithelial cells of the proximal tubule, in the initiation of fibrosis. We recently examined the regulation of HA synthesis by renal PTC *in vitro* under conditions that mimic the diabetic state (10). These studies demonstrate that exposure of PTC to elevated D-glucose concentrations leads to nuclear factor- κ B (NF- κ B)-dependent transcriptional activation of the HA synthase HAS2 and stimulation of HA synthesis. Similarly, HA synthesis is stimulated by addition of the proinflammatory cytokine IL-1 β . We have also characterized PTC expression of the HA receptor CD44 and demonstrated that stimuli inducing HA synthesis by PTC also regulate PTC-HA interactions, with increased binding and internalization resulting from posttranslational modification of CD44 by O-glycosylation (11). The functional significance of alterations in HA synthesis in the renal tubulointerstitium are however unclear. *In vitro*, HA oligosaccharides induce PTC chemokine and leukocyte adhesion molecule expression (12,13). These findings suggest a role for HA in the pathogenesis of renal interstitial inflammation. Inflammatory cell infiltrate, particularly monocyte/macrophage infiltrate, has been implicated in the pathogenesis of a wide diversity of renal diseases (14–16). Understanding the mechanism by which HA mediates inflammatory cell recruitment and its regulation, therefore, has important relevance to kidney disease. The first aim of

Received October 21, 2003. Accepted February 23, 2004.

Correspondence to Dr A. O. Phillips, Institute of Nephrology, University of Wales College of Medicine, Heath Park, Cardiff CF14 4XN. Phone: 44-1222-748411; Fax: 44-1222-748470; E-mail: PhillipsAO@cf.ac.uk

1046-6673/1505-1199

Journal of the American Society of Nephrology

Copyright © 2004 by the American Society of Nephrology

DOI: 10.1097/01.ASN.0000125619.27422.8E

the work presented in the current study was to examine the role of HA in monocyte binding by PTC.

Bone morphogenic protein-7 (BMP-7) is a member of the transforming growth factor- β (TGF- β) superfamily that is required during embryogenesis for normal kidney development (17). Its expression in the kidney has been suggested to be decreased in response to injury (18,19). Furthermore, administration of BMP-7 in models of chronic and acute renal failure results in a reduction of renal interstitial injury (20,21). The

second aim of this study was therefore to examine the effect of BMP-7 on HA generation by PTC and to determine how this affects PTC monocyte interactions.

Materials and Methods

Cell Culture

All experiments were done using HK-2 cells (CRL-2190; American Type Culture Collection [ATCC], Rockville, MD), which are human proximal tubular epithelial cells immortalized by transduction

Table 1. Sequence of oligonucleotide primers

Gene	Primer Sequence	Product Size
β -Actin	F = 5'-CCTTCCTGGGCATGGAGTCCT-3' R = 5'-GGAGCAATGATCTTGATCTT-3'	204 bp
HAS2	F = 5'-GCAGGCGGAAGAAGGGACAAC-3' R = 5'-TCAGGCGGATGCACAGTAAGGA-3'	313 bp
HAS 3	F = 5'-AGTGCAGCTTCGGGGATGA-3' R = 5'-TGATGGTAGCAATGGCAAAGAT-3'	453 bp
Hyal1	F = 5'-CAGGCGTGAGCTGGATGGAGA-3' R = 5'-GTATGTGCAACACCGTGTGGC-3'	400 bp
Hyal2	F = 5'-GAGTTCGCAGCACAGCAGTTC-3' R = 5'-CACCCAGAGGATGACACCAG-3'	446 bp

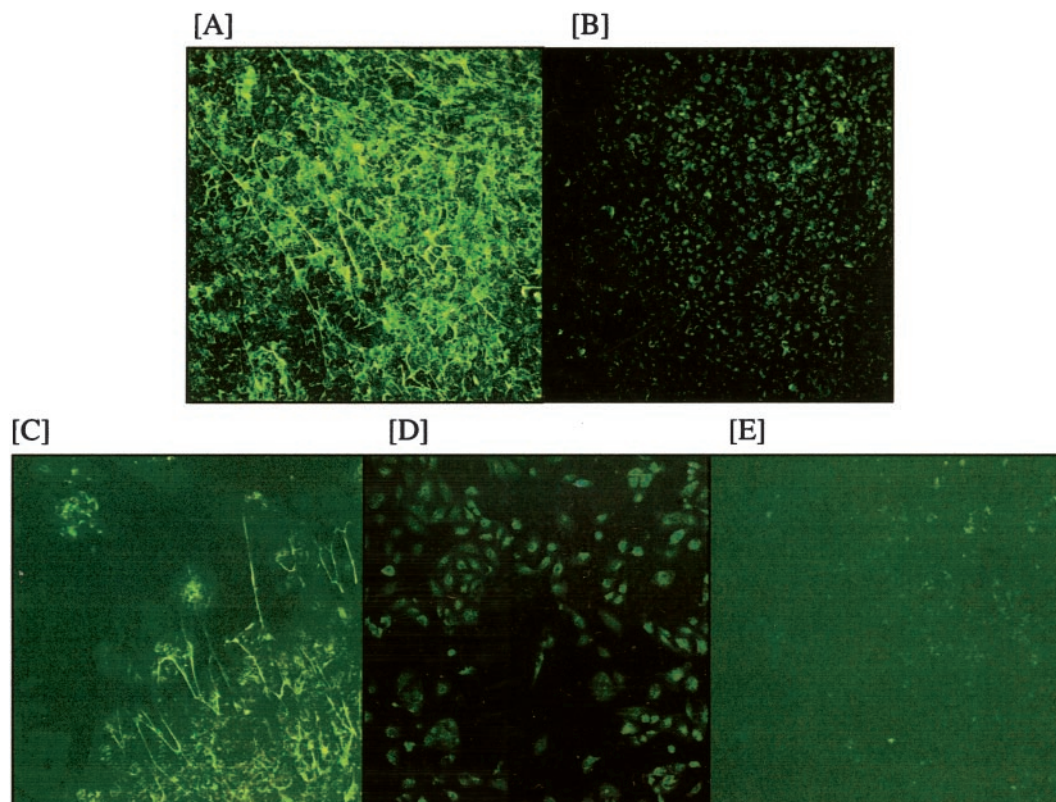


Figure 1. Expression of hyaluronan (HA) on HK2 cells. Confluent (A and B) or subconfluent (C and D) monolayers of HK2 cells were serum-deprived for 48 h before fixation with methanol and detection of HA by addition of biotinylated HA-binding protein. Sections were imaged by confocal microscopy ($\times 10$ objective). To confirm the nature of HA staining in parallel experiments, cells were treated with bovine testicular hyaluronidase (final concentration, 200 $\mu\text{g}/\text{ml}$) at 37°C for 5 min before fixation and addition of biotinylated HA-binding protein (B and D). Specificity of testicular hyaluronidase was confirmed by removal of cell surface HA using 1 U of Streptomyces hyaluronidase before visualization of HA (E). Magnification, $\times 40$.

with human papilloma virus 16 E6/E7 genes (22). Cells were cultured in Dulbecco Modified Eagle Medium/Ham's F12 (Life Technologies, Paisley, UK) supplemented with 10% fetal calf serum (FCS; Biologic Industries Ltd., Cumbernauld, UK), L-glutamine, insulin, transferrin, sodium selenite, hydrocortisone, and Hepes pH 7.2 (Sigma-Aldrich, Poole, UK). Fresh growth medium was added to cells every 3 to 4 d until confluent. All experiments were performed using cells at passage 30 or below, and cells were growth arrested in serum-free medium for 48 h before use in experiments. All experiments were done in serum-free conditions.

U937 cells, originally derived from a human histiocytic lymphoma, were procured from the ATCC. The cells were grown in suspension culture in RPMI medium supplemented with L-glutamine and penicillin/streptomycin and containing 5% FCS. Cells were routinely subcultured at a 1:5 ratio three times per week. Although U937 cells are known to express some macrophage-like characteristics, cell binding was also assessed using human mononuclear cells prepared by dextran sedimentation and Ficoll-paque density separation, as described previously (23), to ensure general applicability of the results obtained using the U937 cells.

Immunocytochemistry

Immunocytochemistry was done on cells grown in eight-well glass chamber slides (Nunc; Life Technologies/BRL Life Technologies Ltd, Paisley, UK). Cells were grown to confluence and stimulated under serum-free conditions with either BMP-7 (Creative Biomolecules, Boston, MA) or IL-1 β (R&D Systems Europe Ltd, Abingdon, UK) for 24 h. In control experiments, cells were incubated in serum-free medium alone. Culture medium was subsequently removed, and the cell monolayer washed with sterile phosphate-buffered saline (PBS). Cells were fixed by addition of 100% ice-cold methanol for 15 min at -20°C and permeabilized with 0.3% Triton X-100 for 30 min. Cells were blocked after fixation with 50% FCS for 1 h before a further washing step with PBS. For HA staining, a biotinylated HA-binding protein (b-HABP; 5 $\mu\text{g}/\text{ml}$) was then added (Seikagaku Corporation, Tokyo, Japan). For U937 staining, a purified monoclonal mouse anti-human CD68 antibody (Pharmingen: Becton Dickenson, Cowley, UK) was used (5 $\mu\text{g}/\text{ml}$). Slides were incubated with b-HABP and anti CD68 antibody at 4°C overnight. The slides were washed with PBS before incubation with fluorescence avidin-D (20 $\mu\text{g}/\text{ml}$; Vector Lab-

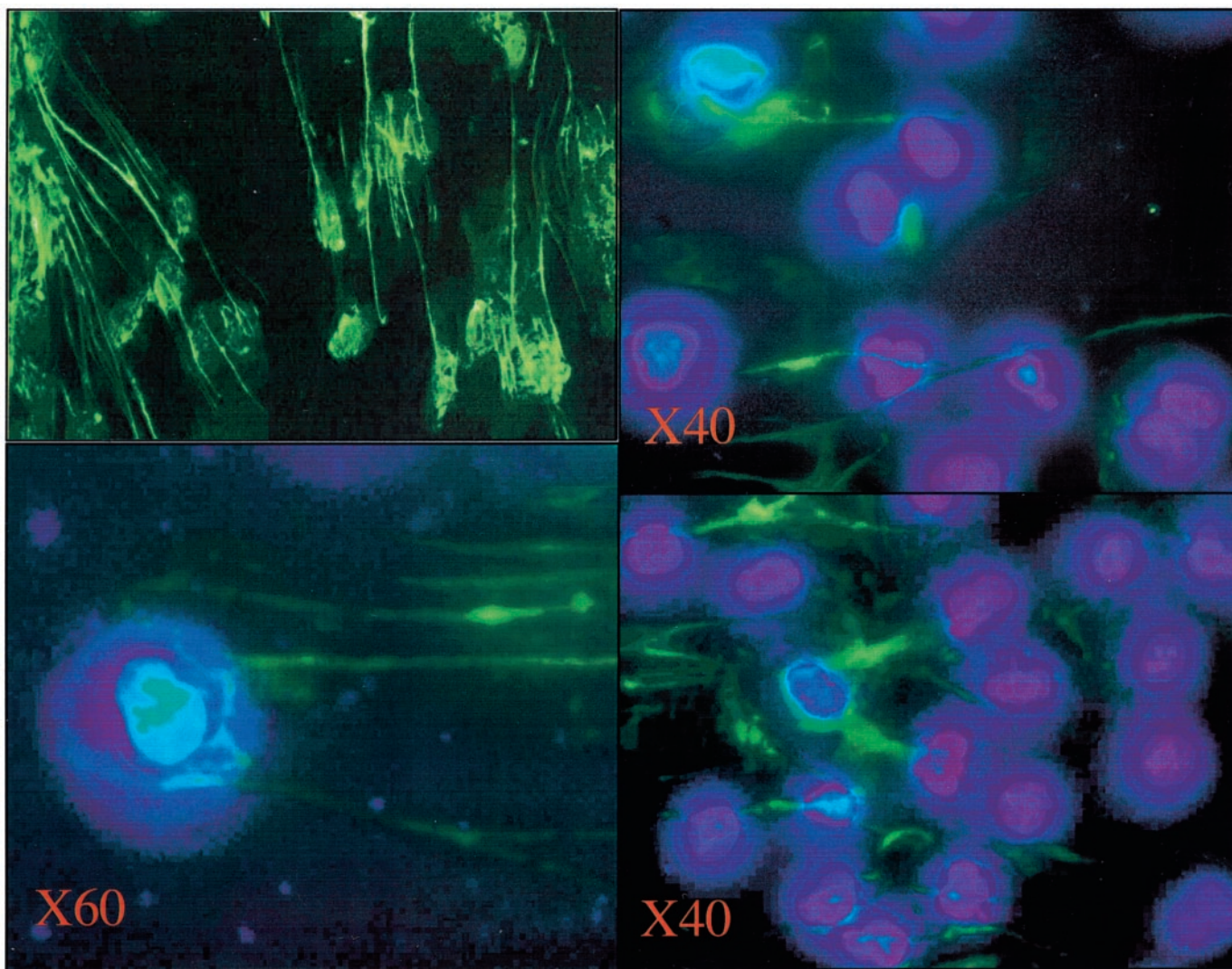


Figure 2. High-power confocal image (A) and fluorescence light microscopic (B, C, and D) images of HA cables in monolayers of HK2 cells. For light microscopic images, HK2 cell nuclei were enhanced by staining of cell nuclei with DAPI.

oratories, CA) used for visualization of b-HABP and 20 $\mu\text{g/ml}$ of Alexa Fluor 568 rabbit anti-mouse IgG (Molecular Probes, Eugene, OR) used for visualization of CD68, at room temperature for 1 h. After a final washing step, specimens were affixed to the slides in Vectasheild mounting medium (Vector Laboratories) and analyzed by confocal laser scanning microscopy (TCS-40 Leica Microsystems, Cambridge UK).

Assay for Leukocyte Adhesion

U937 cell adhesion was measured as described previously (24). Briefly, HK-2 cells were grown on 24-well culture plates until confluent. Stimuli were added to the cells 24 h before the assay. On the day of assay, U937 cells (up to 70×10^6 cells/ml) were labeled for 90 min at 37°C with 100 μCi ^{51}Cr as sodium chromate (Amersham BioSciences, Chalford St Giles, UK). The labeled cells were washed

three times with serum-free culture medium, counted on a hemacytometer, and resuspended to 10^6 viable cell/0.5 ml (as determined by Trypan blue dye exclusion). Incubation medium was removed from HK-2 cultures, and 10^6 monocytes were added to each well. The binding phase of the assay was done at 37°C for 1 h. All cultures were washed with cold medium before lysis by 1% Triton X-100. An aliquot was subsequently removed for quantitation of radiolabel. The number of the U937 cells bound per well was calculated from the initial specific activity (cpm/cell). Spontaneous release of chromium from U937 cells in control incubations without HK-2 cells was typically less than 10%.

The relationship between HK-2 cells and added monocytes was also visualized by light microscopy after 4',6-diamidino-2-phenylindole dihydrochloride hydrate (DAPI, Sigma-Aldrich) staining of cell nuclei. DAPI, at a final concentration of 5 $\mu\text{g/ml}$, was added to the

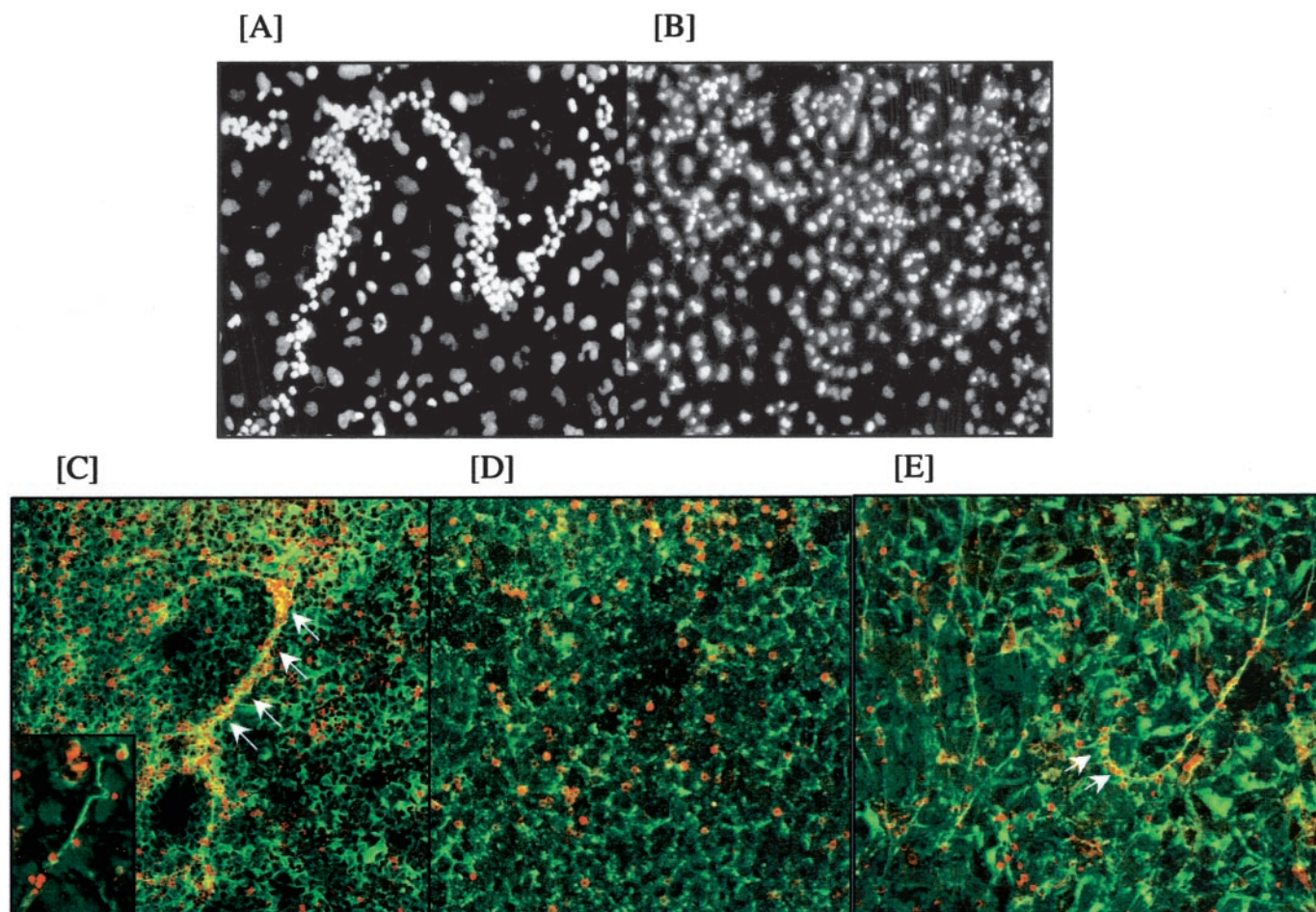


Figure 3. HA cables on confluent monolayers of HK2 cells bind unstimulated monocytes. Confluent monolayers of HK2 cells were serum-deprived for 48 h before addition of 2.5×10^5 unstimulated U937 cells at 37°C for 1 h before fixation. Localization of monocytes was enhanced by staining of cell nuclei with DAPI (A and B; $\times 20$ objective). Binding of monocytes in chain-like configurations can be seen (A). This was abrogated when cells were treated with bovine testicular hyaluronidase (final concentration, 200 $\mu\text{g/ml}$) at 37°C for 5 min before addition of monocytes (B). In parallel experiments, U937 cells were added to confluent monolayers of unstimulated HK-2 cells. HA (green) and monocytes (red) were visualized by addition of biotinylated HA-binding protein and anti-CD68 antibody, respectively, insert demonstrates binding of human peripheral mononuclear cells (C). Double-immunostaining was also performed after treatment of monolayers with bovine testicular hyaluronidase (final concentration, 200 $\mu\text{g/ml}$) at 37°C for 5 min before addition of monocytes (D). The role of CD44 in monocyte binding was assessed by addition of anti-CD44 antibody (final concentration, 5 $\mu\text{g/ml}$) to monocytes for 1 h at 4°C before their addition to confluent monolayers of unstimulated HK-2 cells in the presence of the anti-CD44 antibody (E). HA and monocytes were visualized by immunocytochemistry and confocal microscopy. (Confocal images, $\times 10$ objective).

slides for 1 h at 4°C before mounting with Vectasheild mounting medium. Slides were stored at 4°C until visualized (within 48 h).

Analysis of ³H-Radiolabelled Hyaluronan

In vitro [³H]-labeling of HA was performed as described previously (25). Briefly, growth-arrested confluent HK-2 cells were stimulated with recombinant IL-1 β or BMP7 in the presence of 20 μ Ci/ml ³H glucosamine (Amersham Biosciences) for 24 h. Supernatant samples were collected and treated with equal volume of 200 μ g/ml pronase (Sigma-Aldrich) for 24 h at 37°C to analyze HA released into the culture medium (CM fraction). The remaining cell monolayers were incubated with 10 μ g/ml trypsin (Sigma-Aldrich) in PBS for 10 min at room temperature to remove pericellular (protein-bound) ³H-HA (PB fraction) before addition of an equal volume of 100 μ g/ml pronase for 24 h at 37°C. Finally, after trypsinization, 100 μ g/ml pronase was added to the cell pellet for 24 h at 37°C to solubilize the remaining cells associated ³H-hyaluronan (CA fraction).

Each of the fractions was subsequently passed over DEAE ion-exchange columns (Amersham Biosciences) equilibrated with 8 M urea (pH = 6) in Bis-Tris buffer. The columns were washed using 8 M urea buffer to remove low-molecular weight (M_w) peptides and unincorporated radiolabel. HA was then eluted with 0.3 M NaCl urea buffer. Equal volumes of eluted HA were then precipitated by 3 volumes of 1.3% wt/vol potassium acetate in 95% ethanol in the presence of 50 μ g/ml of each HA, heparin (Sigma-Aldrich), and chondroitin sulfate (Sigma-Aldrich) as co-precipitants. The precipitated HA was separated into two equal volumes, with one directly resuspended in 4 M guanidine HCl buffer and the other incubated with 1 IU Streptococcal hyaluronidase (ICN Biomedicals, Basingstoke, UK) at 37°C for 24 h before addition of 4 M guanidine HCl buffer pH6. Each sample was run through a Sephacryl S-500 column (Amersham Biosciences) before quantitation of radioactivity. The value of the hyaluronidase-treated portion subtracted from the non-hyaluronidase treated portion was taken as HA associated radioactivity.

Alteration in mRNA Expression

Expressions of mRNAs for HA synthases and hyaluronidases were determined by reverse transcription and the polymerase chain reaction (RT-PCR) using specific oligonucleotide primers (Table 1) as described previously (26). PCR was done for various cycles (28–38) to ensure that amplification was in the linear range of the curve. After PCR, one tenth of the PCR reaction from both test and control (β -actin) product were mixed and separated by flat bed electrophoresis in 3% wt/vol NuSieve GTG agarose gels (Flowgen Instruments Ltd, Sittingbourne, UK), stained with ethidium bromide (Sigma-Aldrich) and photographed. The negatives were scanned using a densitometer (Model 620 video densitometer; Bio-Rad Laboratories Ltd), and the density of the bands were compared with those of the housekeeping gene. Results were expressed as the ratio of the gene of interest to β -actin normalized to the control value (the ratio in the unstimulated cells) of each experiment.

Statistical Analyses

Statistical analysis was performed using the unpaired *t* test, with a value of $P < 0.05$ considered to represent a significant difference. The data are presented as means \pm SD of *n* experiments. For each individual experiment the mean of duplicate determinations was calculated.

Results

Cell Surface HA Exists in Two Forms

Confocal imaging of HK-2 cells was used to examine the organization of HA on the cell surface. HA was identified with a biotinylated preparation of the HA-binding protein and detected with fluorescence avidin-D. Photomicrographs of fixed growth arrested HK-2 cells demonstrated diffusely arranged HA over the cell surface. HA was also identified in cable-like structures that spanned several cell lengths (Figure 1). These cables appear to be composed of coalescing bundles of thinner HA strands originating from neighboring cells. HK-2 cell expression of HA cables was variable, although they were present in both subconfluent and confluent cells (Figure 1, A and C).

Confirmation of the nature of the HA content of the cable structures was sought by treatment of confluent monolayers of cells with bovine testicular hyaluronidase (Sigma-Aldrich) before addition of biotinylated HA-binding proteins. After limited hyaluronidase digestion, we were unable to identify any of the cable-like structures in either confluent or subconfluent cells (Figure 1, B and D). Specificity of testicular hyaluronidase in removing HA-based structures was confirmed in parallel experiments in which confluent monolayers of un-

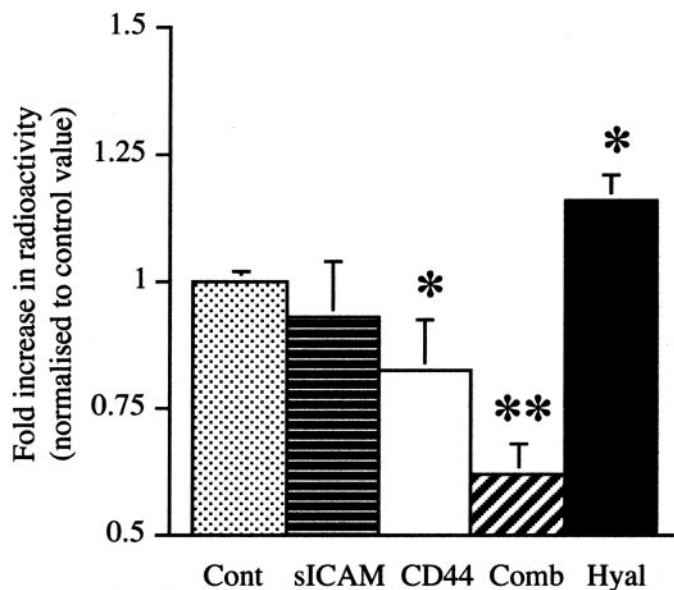


Figure 4. Quantitation of monocyte binding to unstimulated HK-2 cells. In control experiments (Cont), confluent monolayers of serum-deprived HK2 cells were washed with phosphate-buffered saline (PBS) before addition of 1×10^6 ⁵¹Cr chromium-labeled U937 cells again under serum-free conditions for 1 h at 37°C. Quantitation of bound radioactivity was carried out as described in Materials and Methods. Soluble intercellular adhesion molecule (sICAM; 200 ng/ml) or anti-CD44 antibody (CD44; final concentration, 5 μ g/ml) were added to ⁵¹Cr chromium-labeled U937 cells for 1 h at 4°C before their addition to confluent monolayers of unstimulated HK2 cells (in the presence of the antibody), or the monolayer was treated with bovine testicular hyaluronidase (hyal; final concentration, 200 μ g/ml) at 37°C for 5 min before addition of monocytes. Bound radioactivity was subsequently quantified. Data represent mean \pm SD of four individual experiments, * $P < 0.05$.

stimulated cells were treated with 1 U streptomyces hyaluronidase (ICN Biochemicals, OH) before visualization of HA (Figure 1E).

High-power confocal images also demonstrated coalescence of HA cables from numerous cells and suggested an association with the cell nucleus (Figure 2A). Using fluorescence microscopy, HA cables appeared to traverse cells (Figure 2B); by visualization of cell nuclei by staining with DAPI, HA cables could be seen in intimate contact with the nuclear area of cells it traversed (Figure 2, C and D).

Monocytes Bind to Cell Surface Hyaluronan Cables

We used U937 monocytic cells to examine the potential binding capacity of inflammatory cells by HK-2 cells. Unstimulated HK-2 cells bind U937 cells abundantly, as assessed by light microscopy. Cell localization was determined by

DAPI staining of nuclei. Adherent U937 cells appeared as either cells bound individually or cells bound in chains and three-dimensional clumps (Figure 3A).

The relationship between bound U937 cells and HA cable structures was examined by fluorescence confocal microscopy of HA-labeled with biotinylated HA-binding protein and FITC avidin. U937 cells added to monolayers of unstimulated HK-2 cells were detected with anti-CD68 monoclonal antibody. The confocal images showed co-localization of the HA cables and the chains of U937 cells (Figure 3C). There was no association between HA and individually bound U937 cells. In addition, human mononuclear cells isolated from peripheral blood also bound the HA cables (Figure 3C, insert). Pretreatment of HK-2 cell monolayers with bovine testicular hyaluronidase before addition of U937 cells prevented U937 binding in chain like configurations, although binding of scattered individual cells

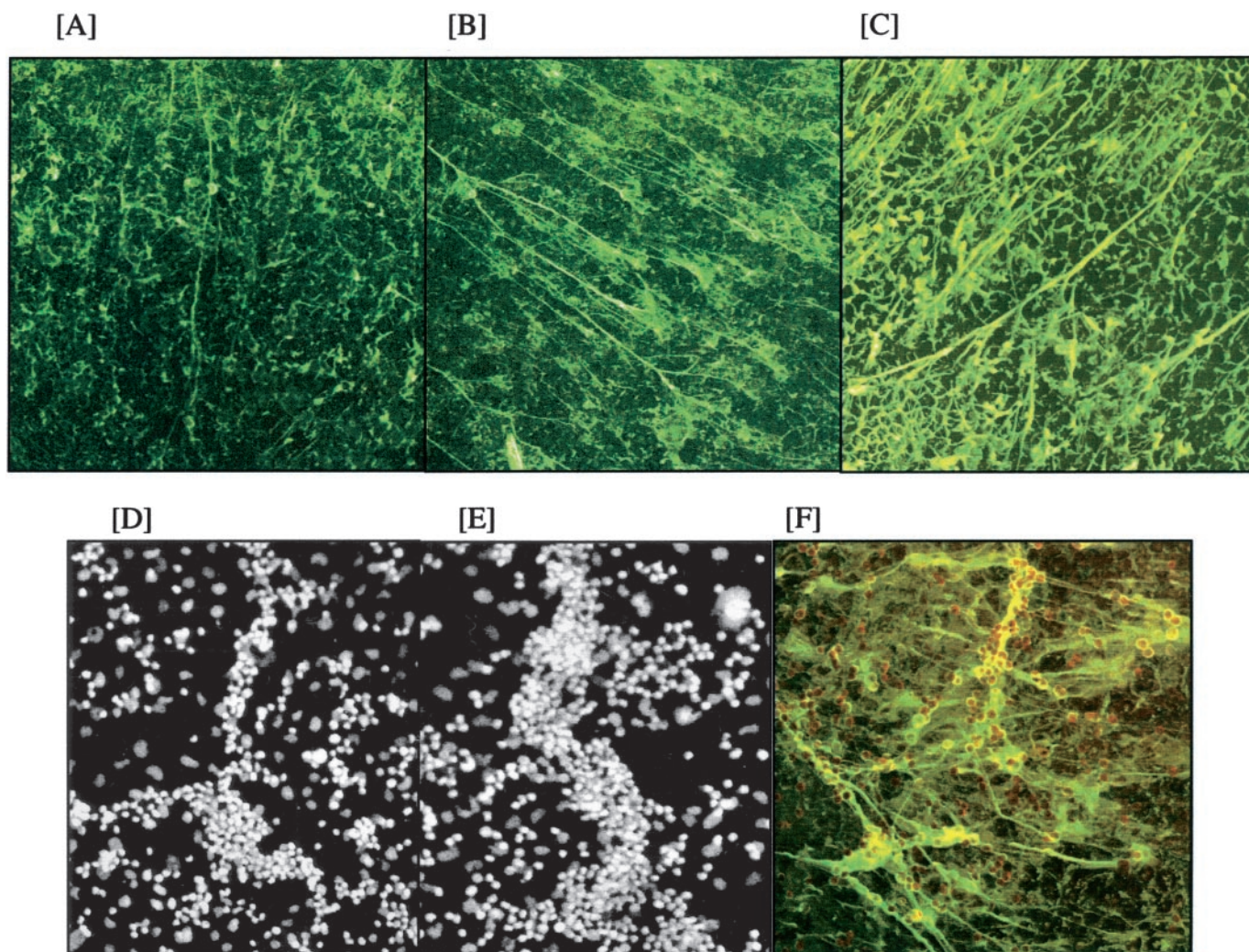


Figure 5. Induction of HA cables and monocyte binding by bone morphogenic protein-7 (BMP-7). After 48 h of serum deprivation, BMP-7 (400 ng/ml) was added to confluent monolayers of HK2 cells for 24 h under serum-free conditions (B and C). In control cultures, cells were exposed to serum-free medium alone (A). After fixation, HA was visualized by addition of biotinylated HA-binding protein and confocal imaging ($\times 10$ objective). In parallel experiments after BMP-7 stimulation, the monolayers were washed before addition of unstimulated U937 cells (2.5×10^5 cells). Monocytes were visualized both by staining of cell nuclei with DAPI (D&E; $\times 20$ objective), and double immunocytochemistry using biotinylated HA-binding protein and anti CD68 antibody (F; $\times 15$ objective).

was not affected. This was demonstrated both by light microscopic pictures taken after DAPI staining (Figure 3B) and also following immunocytochemistry using biotinylated HA-binding protein and anti-CD68 antibody (Figure 3D). Similarly when cell monolayers were treated with testicular hyaluronidase after the addition of the monocytes, no binding of monocytes in chain-like configuration and no HA cables were seen (data not shown). It has been previously suggested that monocytes may interact with HA via monocyte cell surface CD44 (27). Incubation of U937 cells together with unstimulated HK-2 monolayers, in the presence of a human monoclonal blocking antibody to CD44 (Clone B52; The Binding Site, Birmingham, UK), markedly decreased binding of monocytes to HA cables (Figure 3E). Formation of HA cables was unaffected by the addition of the CD44 antibody, as was the binding of monocytes as individual cells.

The nature of monocyte-PTC interaction was further examined by addition of radiolabeled monocytes to unstimulated confluent monolayers of HK2 cells (Figure 4). Bound radioactivity was reduced by either addition of soluble intercellular adhesion molecule (ICAM; R&D Systems Europe Ltd) or addition of CD44 antibody to the monocytes, although this was only statistically significant after CD44 blockade. Combined blockade of both ICAM and CD44 further reduced monocyte binding, thus suggesting that both HA-based interactions and ICAM-dependent interactions contribute to monocyte binding under unstimulated conditions. In contrast to the effect of CD44 blockade, removal of the HA cables by incubation with hyaluronidase before the addition of radiolabeled monocytes led to a significant increase in bound radioactivity, thus suggesting that HA cable-dependent monocyte binding may limit or block monocyte binding to cell surface ICAM.

BMP-7 Stimulates HA Cable Formation

Addition of BMP-7 to confluent monolayers of HK-2 cells led to a marked increase in cell surface HA-based cable structures as assessed by confocal imaging of HA (Figure 5, B and C). The functional significance of the increase in HA cables was assessed by addition of U937 cells to BMP-7-stimulated HK-2 cells. U937 cell binding was examined by fluorescence microscopy and quantified by determination of bound radioactivity after addition of ^{51}Cr -labeled U937 cells.

Examination by fluorescence microscopy demonstrated increased numbers of monocytes bound in chain-like configurations (Figure 4D) and also suggested thicker aggregations of monocytes in these cables (Figure 4E). Double immunocytochemistry confirmed co-localization of HA cables (green) and U937 cell chains (red) (Figure 4F). As with the unstimulated cells, pretreatment of BMP-7 stimulated monolayers of cells with hyaluronidase before the addition of U937 cells removed HA cables and also abrogated binding of U937 cells in chain-like configurations, although binding of individual cells was still seen (data not shown).

Quantitation of monocyte binding, after stimulation with BMP-7 for 24 h, confirmed that there was a significant increase in bound U937 cells at all doses of BMP-7 added (Figure 6A). After stimulation with BMP-7 (200 ng/ml), this represented a 118% increase of bound U937 cells over control; for 800 ng/ml BMP-7, it represented a 160% increase ($P = 0.0001$ for both). The increase in monocyte binding after stimulation with BMP-7 was attenuated by addition of monocytes in the presence of the blocking antibody to CD44 (Figure 6B).

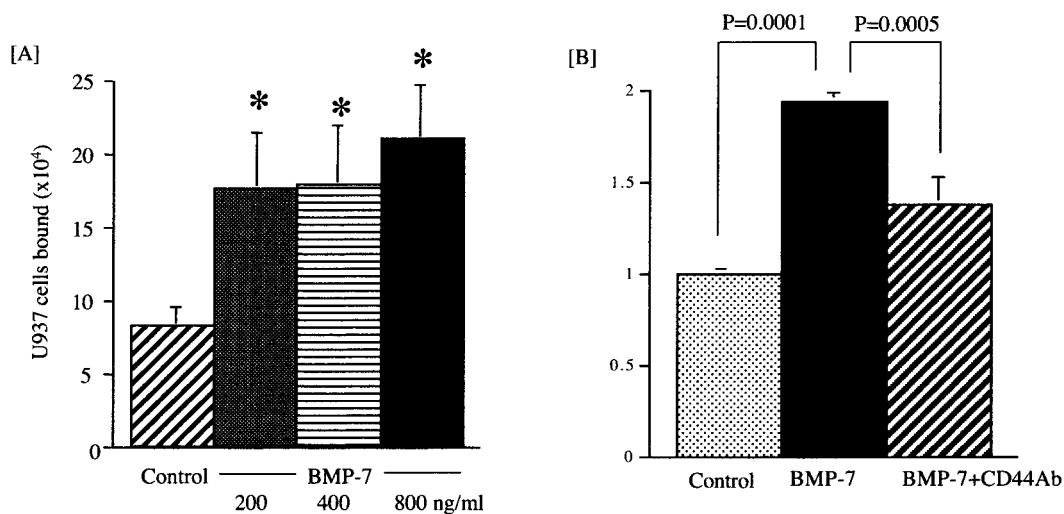


Figure 6. Quantification of monocyte binding after BMP7 stimulation. Confluent monolayers of HK-2 cells were stimulated with increasing doses of BMP-7 (0 to 800 ng/ml) under serum-free conditions for 24 h (A). At the end of the stimulation period, the monolayer was washed with PBS before addition of 1×10^6 ^{51}Cr chromium-labeled U937 cells again under serum-free conditions for 1 h at 37°C. Quantitation of bound radioactivity was carried out as described in Materials and Methods. Parallel experiments were performed to determine the role of CD44 in BMP-7-mediated monocyte binding (B). Cells were stimulated with 400 ng/ml BMP-7 for 24 h. Anti-CD44 antibody (final concentration, 5 $\mu\text{g}/\text{ml}$) was added to ^{51}Cr chromium-labeled U937 cells for 1 h at 4°C before their addition to confluent monolayers of stimulated HK2 cells. Bound radioactivity was subsequently quantified. Data represent mean \pm SD of four individual experiments, * $P < 0.05$.

IL-1 β Induced HA Synthesis But Does Not Increase HA Cable Formation

We have previously demonstrated that IL-1 β is a potent stimulus for HA synthesis as assessed by quantitation of HA in the cell culture supernatant of IL-1 β -treated PTC (10). We therefore sought to determine the effect of IL-1 β on HA cable formation and monocyte binding in HK2 cells.

Stimulation of monolayers of HK-2 cells with IL-1 β led to a dose-dependent increase in binding of ^{51}Cr -labeled U937 cells. IL-1 β -stimulated adhesion was significantly greater than binding of ^{51}Cr -labeled U937 cells to control monolayers of HK-2 cells at all doses. IL-1 β at a dose of 1 ng/ml induced a 45% increase in bound U937 cells over control ($P = 0.0012$); at the highest dose of IL-1 β used (100 ng/ml), a 76% increase in bound U937 cells was seen ($P = 0.0001$) (Figure 7A). In contrast to BMP-7-induced adhesion, IL-1 β -induced monocyte binding was not affected by the addition of a blocking antibody to CD44 (Figure 7B). Addition of monocytes to IL-1 β -stimulated monolayers of HK-2 cells in the presence of soluble ICAM resulted in inhibition of the IL-1 β -induced increase in monocyte binding (Figure 7B). Additionally, examination of HA in IL-1 β -treated and -untreated control cultures by confocal microscopy did not demonstrate any increase in the formation of HA cables (Figure 8C), but it suggested a reduction in cable formation compared with control (Figure 8A). Fluorescence microscopic examination of IL-1 β -stimulated monolayers demonstrated binding of individual U937 cells but no binding in chain-like configurations (Figure 7D).

Characterization of HA after BMP7 or IL-1 Stimulation

Characterization of HA synthesis after either BMP-7 or IL-1 β stimulation was performed by addition of [^3H] glucosamine to cells at the time of stimulation to generate ^3H -labeled HA. Supernatant samples were collected to analyze HA released into the culture medium (CM fraction). The remaining cell layer was treated with trypsin to remove pericellular (protein-bound) ^3H -HA (PB fraction). Finally, the cell pellet after trypsinization was subjected to exhaustive protease digestion to solubilize the remaining cells-associated ^3H -HA (CA fraction). The hydrodynamic size of the synthesized HA in each fraction was subsequently analyzed under dissociative conditions on Sephacryl S-500. The presence of HA in samples was confirmed by incubation with *Streptomyces hyaluronidase*.

Analysis on Sephacryl S-500 of the samples from control HK-2 cells demonstrated that the majority of the labeled HA in all three extracts (CM, PC, IC fractions) appeared near the void volume and therefore was considered to be of high molecular mass (Figure 9). The cell-associated fraction did contain a smaller peak of lower- M_w HA consistent with a pool of intracellular, partially degraded HA as previously reported (28). After addition of BMP-7, an increase in the amount of radiolabeled HA was seen in the supernatant (CM fraction), the pericellular protein bound PC fractions, and the cell-associated (CA) fractions. The increase in HA was, however, most apparent in the pericellular and cell-associated fractions. Furthermore in the cell-associated fraction, there was an apparent increase in the M_w distribution of the second, lower M_w peak.

After IL-1 β stimulation, there was also an increase in the

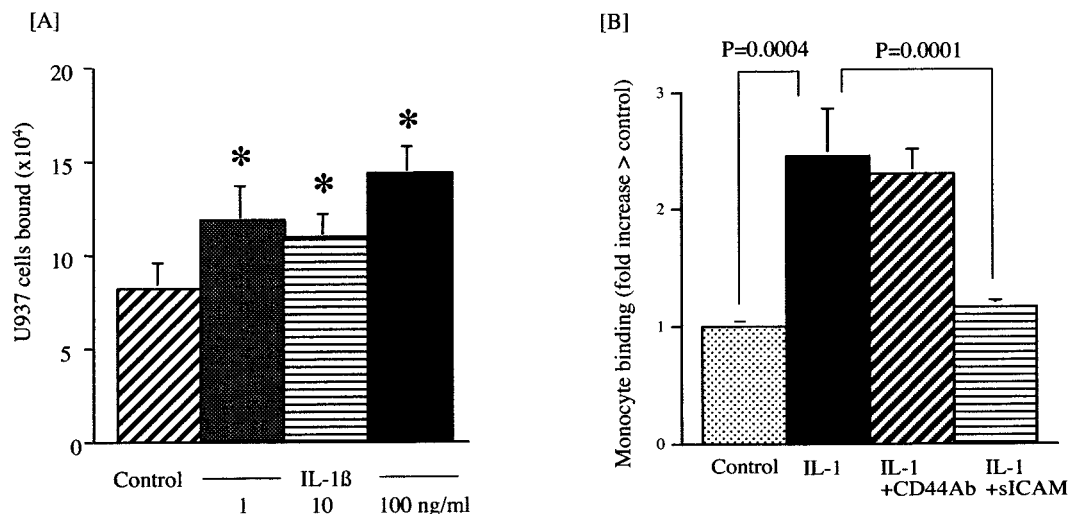


Figure 7. Quantification of monocyte binding after IL-1 β stimulation. Confluent monolayers of HK-2 cells were stimulated with increasing doses of IL-1 β (0 to 100 ng/ml) under serum-free conditions for 24 h (A). At the end of the stimulation period, the monolayer was washed with PBS before addition of 2.5×10^5 ^{51}Cr -labeled U937 cells again under serum-free conditions for 1 h at 37°C. Quantitation of bound radioactivity was carried out as described in Materials and Methods. Parallel experiments were done to determine the role of CD44 and ICAM in IL-1 β -mediated monocyte binding (B). Cells were stimulated with 1 ng/ml IL-1 β for 24 h. Anti-CD44 antibody (final concentration, 5 $\mu\text{g}/\text{ml}$), or soluble ICAM (200 ng/ml) was added to ^{51}Cr -labeled U937 cells for 1 h at 4°C before their addition to confluent monolayers of stimulated HK-2 cells (in the presence of antibody/sICAM). Bound radioactivity was subsequently quantified. Data represent mean \pm SD of four individual experiments, * $P < 0.05$.

amount of HA in all three of the cellular pools. However, in contrast with BMP-7–associated changes, IL-1 β induced the largest change in the high- M_w HA secreted into the cell culture supernatant (Figure 9).

Expression of HA synthases (HAS) mRNA in HK-2 cells was examined by RT-PCR. BMP-7 stimulation led to induction of HAS2 mRNA above that seen in the control cells (Figure 10A). HAS3 mRNA was constitutively expressed by HK-2 cells as previously demonstrated (10) and was not influenced by the addition of BMP-7 (Figure 10B). Examination of hyaluronidase expression was also examined by RT-PCR. After addition of BMP-7, there was a significant decrease in the expression of both HYAL 1 and 2 mRNA (Figure 10, C and D). As we have previously reported, stimulation with IL-1 β also increased the expression of HAS2 mRNA, without affecting expression of HAS 3 mRNA (Figure 10, A and B). In contrast to the effect of BMP-7, stimulation with IL-1 β did not influence expression of either hyaluronidase mRNA (Figure 10, C and D).

Discussion

Although numerous studies have demonstrated increased HA within the kidney cortex associated with disease, the functional significance of these changes is not clear. What is clear is that the traditional view of HA being a structural scaffold is now being revised as it becomes apparent that it may function as a cellular signaling molecule after binding to its cell surface receptors (CD44 and RHAMM) or following internalization via CD-44 mediated endocytosis (29). HA has therefore been implicated in a number of biologic processes, including embryonic development, tumor growth, chronic inflammation, and wound healing (1). Several workers have reported that HA-oligosaccharides may stimulate gene expression and protein synthesis of chemokines (30) and interstitial collagens (31). In contrast, high- M_w HA oligosaccharides inhibit the bioactivity of TGF- β and stimulate the secretion of tissue inhibitors of metalloproteinases (32,33). These observations therefore suggest that high- M_w HA may be “anti-fibrotic,” whereas, if unabated, the generation of low M_w HA fragments may disrupt the normal balance between cells and matrix and contribute to the pathophysiology of chronic tissue inflammation and fibrosis. Fewer data are available on the effect of HA on renal cells

In this article, we have demonstrated that HA mediates binding of monocytes to PTC when HA coalesces into cable-like structures. These structures seem to originate from numerous different cells and form cables spanning several cell widths. HA cables present on unstimulated cells bind unstimulated monocytes, and their formation is upregulated by BMP-7. As a consequence of increased HA cable formation, we have shown that BMP-7 also increased HA-dependent monocyte binding. Increased HA cable formation after addition of BMP-7 was associated with induction of HAS2 mRNA, and an increase in newly synthesized cell associated HA was also observed. This would suggest a specific effect of BMP-7 on the assembly of pericellular HA structures. The inter- α -trypsin inhibitor (I α I) family are a group of serum protease inhibitors,

and previous studies utilizing colonic mucosal smooth muscle cells have suggested that the heavy chains of I α I are critical to the formation HA-based cables (34). It was particularly noted that there was a marked attenuation of HA cable formation in the absence of serum. All our experiments were performed in the absence of serum. However, we have previously demonstrated that PTC express bikunin and H3 components of the I α I family constitutively (35). This may therefore explain the ability of PTC to generate stable HA-based cable structures in the absence of serum components.

The specificity of the effect of BMP-7 was confirmed by data demonstrating that IL-1 β , despite being a potent stimulus of HA synthesis, was unable to alter HA cable formation. IL-1 β did however increase monocyte binding. This increase appeared to be unrelated to any alteration in formation of HA cables, but rather monocyte binding to the HK-2 cells was mediated by other leukocyte adhesion molecules, particularly ICAM. Importantly, these data provide evidence that not only the quantity, but also the structure of HA is crucial for leukocyte binding.

An important difference between BMP-7 and IL-1 β in terms of their impact on HA turnover was their effect on hyaluronidase expression. We were able to demonstrate downregulation of hyaluronidase (hyal1 and hyal2) at the level of transcription

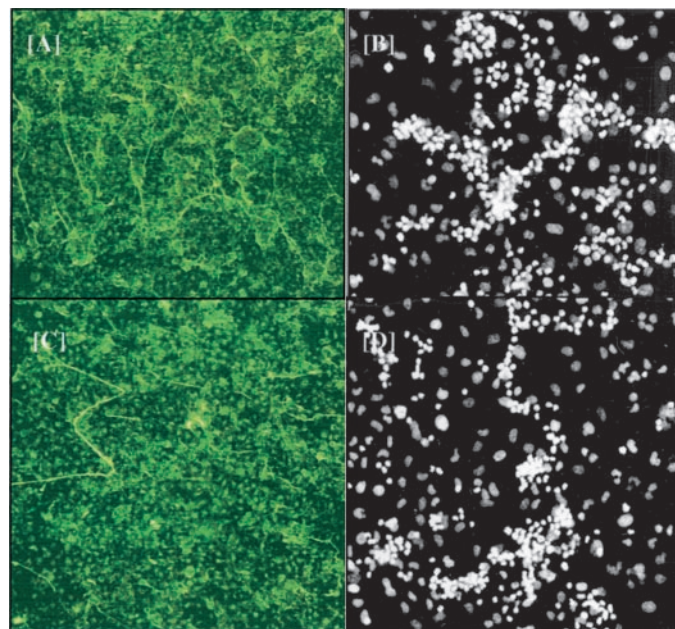


Figure 8. Visualization of HA and monocyte binding in control cells (A and B) and after IL-1 β stimulation (C and D). After 48 h of serum deprivation, IL-1 β (1 ng/ml) was added to confluent monolayers of HK2 cells for 24 h under serum-free conditions. In control experiments, cells were exposed to serum-free medium alone. After fixation, HA was visualized by addition of biotinylated HA-binding protein and confocal imaging (A and C; $\times 10$ objective). In parallel experiments after IL-1 β stimulation, the monolayers were washed before addition of unstimulated U937 cells (2.5×10^5 cells). In both IL-1 β -stimulated (D) and control (B) monolayers, monocytes were visualized by staining of cell nuclei with DAPI-blue ($\times 20$ objective).

with BMP-7, whereas IL-1 β did not alter their expression. The change in the M_w of the cell-associated HA after stimulation with BMP-7 is consistent with decreased intracellular degradation of HA due to reduced hyaluronidase activity. As yet, there are no antibodies available to confirm that this was also paralleled by a decrease in protein expression and enzyme activity, but it is interesting to speculate that this difference between BMP-7 and IL-1 β -mediated regulation of hyaluronidase may be a key in understanding their differential effects on HA cable formation. HA synthesis occurs at or close to the cell membrane, and the growing HA chain is extruded through the membrane into the extracellular space (36). We postulate that downregulation of hyaluronidase activity by BMP-7 allows HA to remain associated with HAS and that HA extruded through the cell membrane is anchored to HAS isoforms and

associates with similarly anchored HA from neighboring cell thus forming cables. In contrast, when hyaluronidase activity is not decreased, as seen after addition of IL-1 β , extruded HA is cleaved at the cell surface and secreted into the surrounding environment. In our studies, this is reflected by the increased concentration of HA in the culture supernatant after addition of IL-1 β , while BMP-7 led to a much smaller increase of HA in the culture supernatant, presumably due to less HA cleavage and release.

Although BMP-7 was originally identified as a protein that induced bone and cartilage formation, with an important role in the morphogenesis of embryo and in postnatal life (37), it is also produced in kidney (37,38). Recent studies have shown that BMP-7 is able to prevent kidney damage *in vivo* in numerous animal models of disease. In models of renal isch-

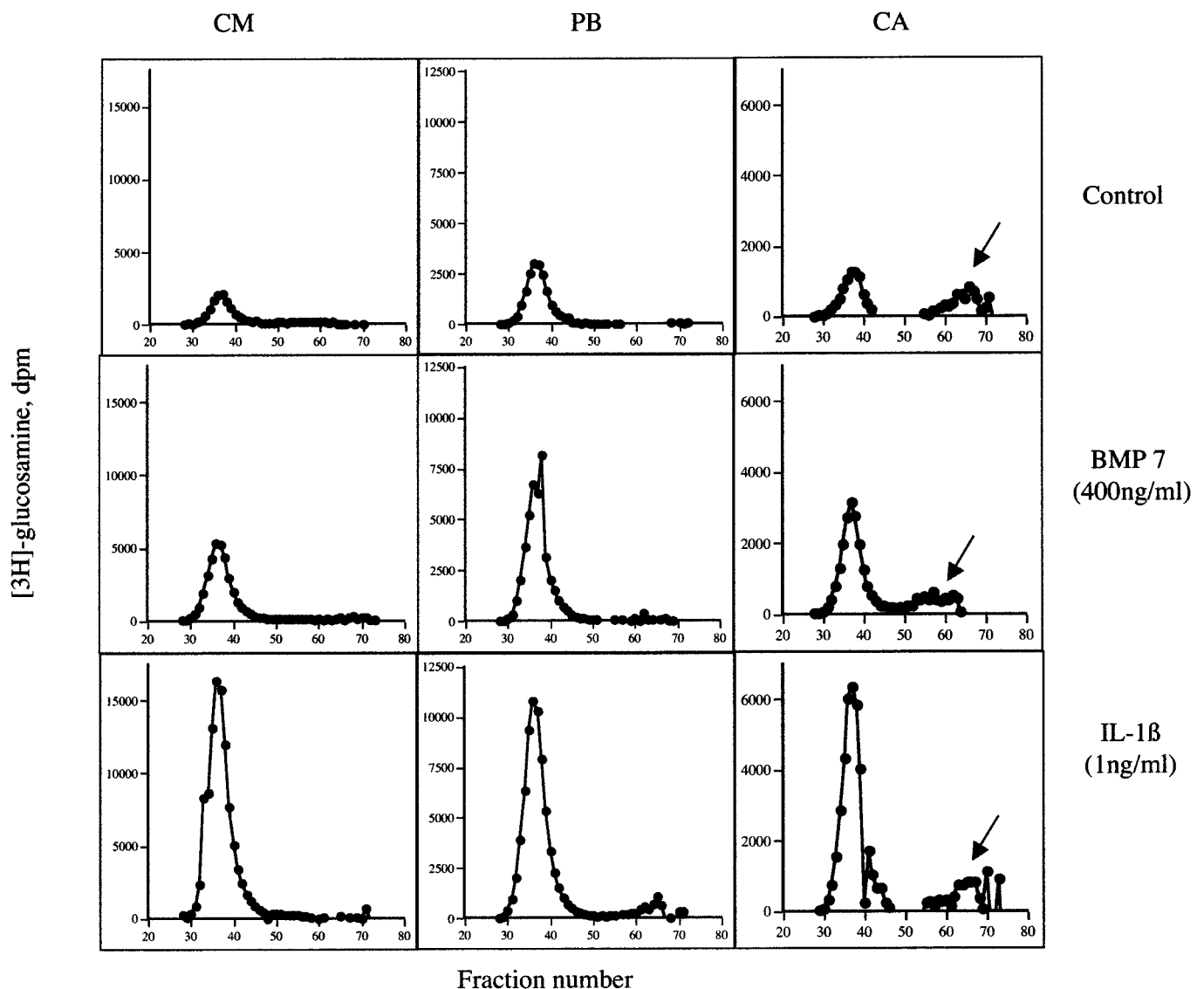


Figure 9. Analysis of ^3H radiolabeled hyaluronan (HA). Confluent serum-deprived monolayers of HK-2 cells were stimulated with BMP-7 (400 ng/ml) or IL-1 β (1 ng/ml) or exposed to serum-free control conditions as indicated for 24 h in the presence of 20 $\mu\text{Ci/ml}$ [^3H] glucosamine. Subsequently, conditioned medium (CM) and protein-bound (PB) and cell-associated (CA) HA fractions were prepared as described in Materials and Methods. Radiolabeled HA was subsequently analyzed by Sephacryl S-500 chromatography.

emia, infusion of BMP-7 reduces severity of renal injury and suppresses inflammation by downregulation of intercellular adhesive molecules (20). Interstitial inflammation and fibrogenesis associated with unilateral ureteral obstruction (UUO) are also prevented *in vivo* by administration of BMP-7 at the time of UUO (21). BMP-7 promoted maintenance of tubular epithelial integrity in the same model. This is consistent with *in vivo* studies demonstrating counteraction of TGF- β 1-induced epithelial-to-mesenchymal transition and reversal of chronic renal injury in the nephrotoxic serum nephritis model (39). Finally in the streptozotocin model of diabetic nephropathy, BMP-7 therapy *in vivo* markedly ameliorated glomerular pathology, decreased tubulointerstitial volume, and reduced proteinuria (40). *In vitro* studies shed some further light on the mechanistic basis of the mode of action of BMP-7. In mesangial cells, it reduces TGF- β 1-induced extracellular matrix ef-

fects (41). Specific membrane-bound high-affinity BMP-7 receptors have also been characterized on adult rat kidney tubular cells (42), and *in vitro* in PTC, BMP-7 antagonizes TNF- α -stimulated increases in expression of proinflammatory cytokines and chemokines (43). How then can we relate the anti-inflammatory and antifibrotic effects of BMP-7 with increased HA cable-mediated monocyte binding?

Binding interactions between leukocytes and other cells are best characterized in endothelial cells in which leukocyte integrins on their surface bind to their ligands such as ICAM-1 and VCAM-1 (members of the Ig super-family) (44). Similar mechanisms of binding have been demonstrated in resident renal cells such as PTC (45) and fibroblasts (23). Proximal tubular cells express the adhesion molecules ICAM-1 and VCAM-1, and upregulation of these adhesion molecules predict outcome in inflammatory renal disease (45). Interaction of

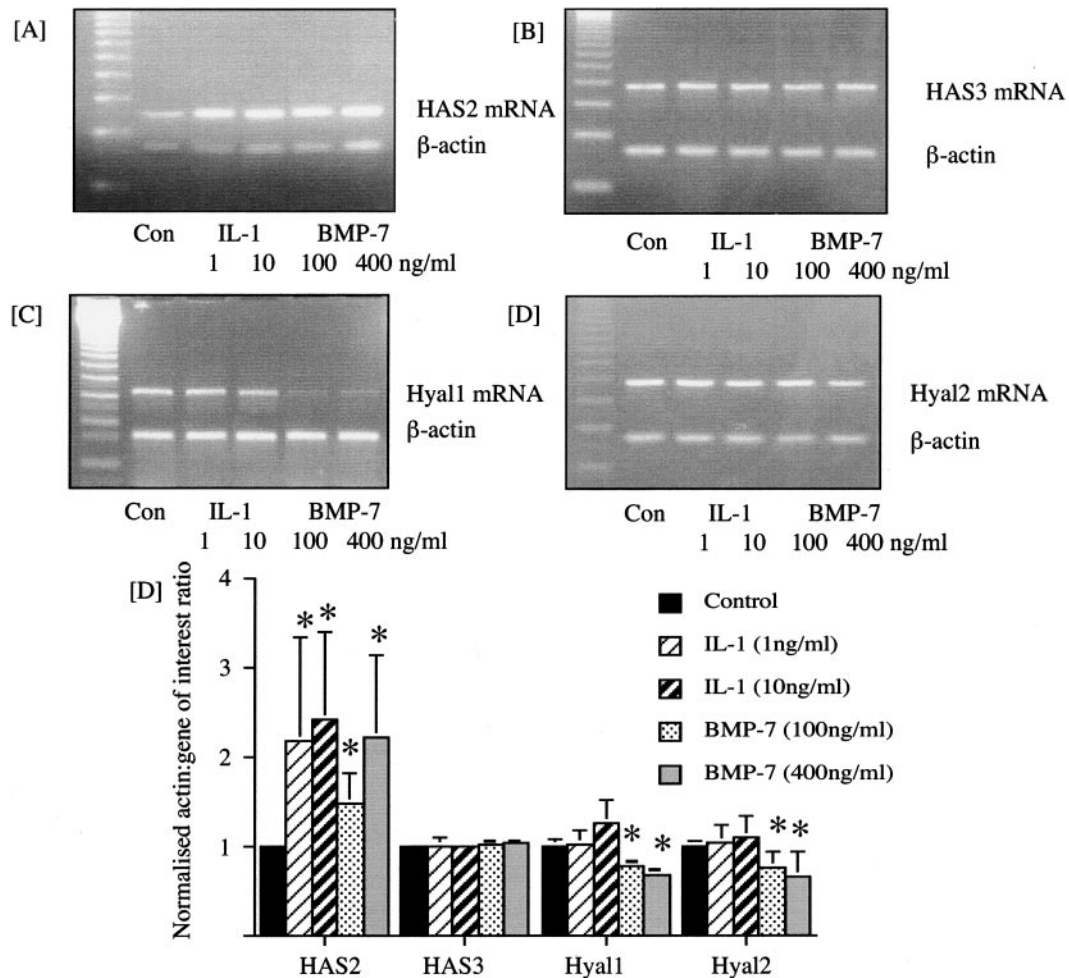


Figure 10. Expression of HA synthases (HAS2 and HAS3) mRNA and hyaluronidase (Hyal1 and Hyal2) mRNA. Confluent monolayers of HK-2 cells were stimulated with either IL-1 β (1 ng/ml) or increasing doses of BMP-7 (0 to 800 ng/ml) for 24 h as indicated. In control experiments, cells were exposed to serum-free medium only (Con). At the end of the experimental period, total cellular RNA was extracted and RT-PCR done as described in Materials and Methods. Ethidium bromide-stained PCR products were separated on a 3% agarose gel. One representative gel of four individual experiments is shown. PCR amplification for 28 cycles for β -actin mRNA, 36 cycles for HAS2 mRNA (A), 36 cycles for HAS3 mRNA (B), 36 cycles for Hyal1 mRNA (C), and 32 cycles for Hyal2 mRNA (D). Densitometric ratios, normalized to the control value, of each of the genes of interest compared with the housekeeping gene, β -actin, of four individual experiments are shown in panel E. Data represents mean \pm SD, * P < 0.05 compared with the mean control ratio for each experiment.

infiltrating inflammatory cells with PTC through these adhesion molecules stimulate the generation of several cytokine cascades (46). It is likely that such as inflammatory loops, if not controlled appropriately, will turn into a chronic phase which leads to the development of progressive fibrosis characteristic of chronic renal disease. In this article, we have demonstrated that BMP-7–induced monocyte binding is distinct from IL-1 β –induced monocyte binding. We postulate that the HA cables keep the monocytes away from the proinflammatory receptors. This hypothesis is supported by demonstration of increased monocyte binding to unstimulated cells when HA cables were removed by hyaluronidase treatment before the addition of the U937 cells. In addition, previous studies have suggested that BMP-7 may also influence ICAM–leukocyte interaction by downregulation of ICAM expression in PTC (43). In an *in vivo* setting, this would reduce the impact of any infiltrating monocytes and prevent the development of a proinflammatory amplification loop, which may lead to progressive interstitial fibrosis.

This effect of cell-associated HA cables in which HA is predominantly of high M_w is in marked contrast to the reported effects of soluble low- M_w HA. Addition of low- M_w HA is a potent stimulus for increased expression of ICAM-1 and VCAM-1 in tubular epithelial cells (13). Together with increased expression of chemokines after addition of fragmented HA to PTC (12), this suggests that secreted HA, particularly when partially degraded, enhances leukocyte adhesion and subsequent cell activation, providing an amplification loop for proinflammatory effects of cytokines such as IL-1 β . This reinforces the principle that high- M_w HA generally represents the normal homeostatic state, whereas the generation of low- M_w HA fragments signals a disruption of the normal homeostatic environment.

In conclusion, most renal diseases are characterized by progressive loss of renal function, which results in a pathogenetic mechanism that is independent of the original disease (47). This final common pathway is initially characterized by the triggering of interstitial infiltration of inflammatory cells, which trigger further tubular damage, and interstitial fibrosis, which correlates with the rate of progression of renal disease. This seems to hold true, even in what are considered to be non-inflammatory diseases such as diabetic nephropathy, with recent studies suggesting that macrophage-derived proinflammatory cytokines acting upon resident cells may represent key events in progressive nephropathy (14,48). The data presented in this article provide insight into how alterations in HA synthesis in the renal cortex may be involved in modulation of the interaction between infiltrating inflammatory cells and resident cells and furthermore suggest a mechanism by which the known antiinflammatory and antifibrotic effects of BMP-7 in renal disease may be mediated. We speculate that the presence of BMP-7 is an important determinant of the function of HA. Chronic renal impairment is associated with a relative deficiency of BMP-7 but increased HA in the kidney. Under these conditions, increased HA generation is unlikely to form HA-based cables and therefore may contribute to the damaging fibrotic response. In the presence of BMP-7, however,

the formation of cables is facilitated the consequence of which may be decreased interaction of infiltrating cells with cell surface adhesion molecules on the resident cells.

Acknowledgments

This work was supported by a Grant from Diabetes UK. AOP is supported by a GlaxoSmithKline Advanced Fellowship. The work was presented in abstract form at HA2003.

References

1. Laurent TC, Fraser RE: Hyaluronan. *FASEB* 6: 2397–2404, 1992
2. Hansell P, Göransson V, Odland C, Gerdin B, Hällgren R: Hyaluronan content in the kidney in different states of body hydration. *Kidney Int* 58: 2061–2068, 2000
3. Mahadevan P, Larkins RG, Fraser JRE, Fosang AJ, Dunlop ME: Increased hyaluronan production in the glomeruli from diabetic rats: Link between glucose induced prostaglandin production and reduced sulphated proteoglycans. *Diabetologia* 38: 298–305, 1995
4. Mahadevan P, Larkins RG, Fraser RE, Dunlop ME: Effect of prostaglandin E2 and hyaluronan on mesangial cell proliferation. *Diabetes* 45: 44–50, 1996
5. Sibalic V, Fan X, Loffing J, Würthrich RP: Upregulated renal tubular CD44, hyaluronan, and osteopontin in kdkd mice with interstitial nephritis. *Nephrol Dial Transplant* 12: 1344–1353, 1997
6. Lewington AJP, Padanilam BJ, Martin DR, Hammeramr MR: Expression of CD44 in kidney after acute ischemic injury in rats. *Am J Physiol* 278: R247–R254, 2000
7. Wells A, Larsson E, Hanas E, Laurent T, Hallgren R, Tufvesson G: Increased hyaluronan in acutely rejecting human kidney grafts. *Transplantation* 55: 1346–1349, 1993
8. Wells AF, Larsson E, Tengblad A, Fellstrom B, Tufvesson G, Klareskog L, Laurent TC: The localisation of hyaluronan in normal and rejected human kidneys. *Transplantation* 50: 240–243, 1990
9. Sano N, Kitazawa K, Sugisaki T: Localization and roles of CD44, Hyaluronic acid and osteopontin in IgA nephropathy. *Nephron* 89: 416–21, 2001
10. Jones SG, Jones S, Phillips AO: Regulation of renal proximal tubular epithelial cell hyaluronan generation: Implications for diabetic nephropathy. *Kidney Int* 59: 1739–1749, 2001
11. Jones SG, Ito T, Phillips AO: Regulation of proximal tubular epithelial cell CD44 mediated binding and internalisation of hyaluronan. *Int J Biochem Cell Biol* 35: 1361–1377, 2003
12. Beck-Schimmer B, Oertli B, Pasch T, Würthrich RP: Hyaluronan induces monocyte chemoattractant protein-1 expression in renal tubular epithelial cells. *J Am Soc Nephrol* 9: 2283–2290, 1998
13. Oertli B, Beck-Schimmer B, Fan X, Würthrich RP: Mechanisms of hyaluronan-induced up-regulation of ICAM-1 and VCAM-1 expression by murine kidney tubular epithelial cells: Hyaluronan triggers cell adhesion molecule expression through a mechanism involving activation of nuclear factor - κ B activating protein-1. *J Immunol* 161: 3431–3437, 1998
14. Young BA, Johnson RJ, Alpers CE, Eng CE, Gordon K, Floege J, Couser W: Cellular events in the evolution of experimental diabetic nephropathy. *Kidney Int* 47: 935–944, 1995
15. Lavaud S, Michel O, Sassy-Prigent C, Heudes D, Bariety J, Chevalier J, Belair MF, Mandet C: Early influx of glomerular macrophages precedes glomerulosclerosis in the Obese Zucker Rat model. *J Am Soc Nephrol* 7: 2604–2615, 1996

16. Sassy-Pringent C, Heudes D, Mandet C, Belair MF, Michel O, Perdureau B, Bariety J, Bruneval P: Early glomerular macrophage recruitment in streptozotocin induced diabetic rats. *Diabetes* 49: 466–475, 2000
17. Dudley AT, Lyons KM, Robertson EJ: A requirement for bone morphogenic protein 7 during development of the mammalian kidney and eye. *Genes Dev* 9: 2795–2807, 1995
18. Almanzar MM, Fraszier KS, Dube PH, Piqueras AI, Jones WK, Charette MF, Paredes AL: Osteogenic protein-1 mRNA expression is selectively modulated after acute ischemic renal injury. *J Am Soc Nephrol* 9: 1456–1463, 1998
19. Wang SN, Lapage J, Hirschberg R: Loss of tubular bone morphogenic protein-7 in diabetic nephropathy. *J Am Soc Nephrol* 12: 2392–2399, 2001
20. Vukicevic S, Basic V, Rogic D, Basic N, Shih MS, Shepard A, Jin D, Dattatreyaumurthy B, Jones W, Dorai H, Ryan S, Griffiths D, Maliakal J, Jelic M, Pastorcic M, Stavljenic A, Sampath TK: Osteogenic protein-1 reduces severity of injury after ischemic acute renal failure in rat. *J Clin Invest* 102: 202–214, 1998
21. Hruska KA, Guo G, Wozniak M: Osteogenic protein-1 prevents renal fibrogenesis associated with ureteral obstruction. *Am J Physiol* 279: F130–F143, 2000
22. Ryan MJ, Johnson G, Kirk J, Fuerstenberg SM, Zager RA, Torok-Storb B: HK-2: An immortalized proximal tubule epithelial cell line from normal adult human kidney. *Kidney Int* 45: 48–57, 1994
23. Clayton A, Petit EJ, Halett MB, Steadman R: ICAM-1 dependent binding to renal fibroblasts initiates *de novo* adhesion molecule synthesis. *J Cell Sci* 111: 443–453, 1998
24. de la Motte CA, Hascall VC, Calabro A, Yen-Lieberman B, Strong SA: Mononuclear leukocytes preferentially bind via CD44 to hyaluronan on human interstitial mucosal smooth muscle cells after virus infection or treatment with poly (I. C). *J Biol Chem* 274: 30747–30755, 1999
25. Yung S, Thomas GJ, Davies M: Induction of hyaluronan metabolism after mechanical injury of human peritoneal mesothelial cells in vitro. *Kidney Int* 58: 1953–1962, 2000
26. Phillips AO, Steadman R, Topley N, Williams JD: Elevated D-glucose concentrations modulate TGF- β 1 synthesis by human cultured renal proximal tubular cells: the permissive role of platelet derived growth factor. *Am J Pathol* 147: 362–374, 1995
27. Levesque MC, Haynes BF: In vitro culture of human peripheral blood monocytes induces hyaluronan binding and up-regulates monocyte variant CD44 isoform expression. *J Immunol* 156: 1557–1565, 1996
28. Tammi R, Rilla K, Pienimäki JP, MacCallum DK, Hogg M, Luukkonen M, Hascall VC, Tammi M: Hyaluronan enters keratinocytes by a novel endocytic route for catabolism. *J Biol Chem* 276: 35111–35122, 2001
29. Hua Q, Knudson CB, Knudson W: Internalisation of hyaluronan by chondrocytes occurs via receptor mediated endocytosis. *J Cell Sci* 106: 365–375, 1993
30. McKee CM, Penno MB, Cowman M, Burdick MD, Strieter RM, Bao C, Noble PW: Hyaluronan (HA) fragments induce chemokine gene expression in alveolar macrophages. *J Clin Invest* 98: 2403–2413, 1996
31. Rooney P, Wang M, Kumar P, Kumar S: Angiogenic oligosaccharides of hyaluronan enhance the production of collagens by endothelial cells. *J Cell Sci* 105: 213–218, 1993
32. Yasui T, Akatsuka M, Tobetto K, Umemoto J, Ando T, Yamashita K, Hayakawa T: Effects of hyaluronan on the production of stromolysin and tissue inhibitor of metalloproteinase-1 (TIMP-1) in bovine articular chondrocytes. *Biomed Res* 13: 343–348, 1992
33. Locci P, Marinucci L, Lilli C, Martinese D, Becchetti E: Transforming growth factor β 1 - hyaluronic acid interaction. *Cell Tissue Res* 281: 317–324, 1995
34. de La Motte CA, Hascall VC, Drazba J, Bandyopadhyay SK, Strong SA: Mononuclear leukocytes bind to specific hyaluronan structures on colon mucosal smooth muscle cells treated with polyinosinic acid:polycytidylic acid: inter-alpha-trypsin inhibitor is crucial to structure and function. *Am J Pathol* 163: 121–133, 2003
35. Janssen U, Thomas G, Glant T, Phillips AO: Regulation of inter-alpha-trypsin inhibitor (Ialpha-I) and tumour necrosis factor-stimulated gene 6 (TSG-6) expression in human renal proximal tubular epithelial cells. *Kidney Int* 60: 126–136, 2001
36. Fülöp C, Salustri A, Hascall VC: Coding sequence of a hyaluronan synthase homologue expressed during expansion of the mouse cumulus-oocyte complex. *Arch Biochem Biophys* 337: 261–266, 1997
37. Helder MN, Ozkaynak E, Sampath KT, Luyten FP, Latin V, Oppermann H, Vukicevic S: Expression pattern of osteogenic protein-1 (bone morphogenetic protein-7) in human and mouse development. *J Histochem Cytochem* 43: 1035–1044, 1995
38. Ozkaynak E, Schnegelsberg PN, Oppermann H: Murine osteogenic protein (OP-1): high levels of mRNA in kidney. *Biochem Biophys Res Com* 179: 116–23, 1991
39. Zeisberg M, Hanai J, Sugimoto H, Mammoto T, Charytan D, Strutz F, Kalluri R: BMP-7 counteracts TGF-beta1-induced epithelial-to-mesenchymal transition and reverses chronic renal injury. *Nature Medicine* 9: 964–968, 2003
40. Klahr S, Morrissey J, Hruska K, Wang S, Chen Q: New approaches to delay the progression of chronic renal failure. *Kidney Int* S23–S26, 2002
41. Wang S, Hirschberg R: BMP7 antagonizes TGF-beta -dependent fibrogenesis in mesangial cells. *Am J Physiol* 284: F1006–F1013, 2003
42. Bosukonda D, Shih MS, Sampath KT, Vukicevic S: Characterisation of receptors for osteogenic protein-1/bone morphogenic protein-7 in rat kidneys. *Kidney Int* 58: 1902–1911, 2000
43. Gould SE, Day M, Jones SS, Dorai H: BMP-7 regulates chemokine, cytokine, and hemodynamic gene expression in proximal tubule cells. *Kidney Int* 61: 51–60, 2002
44. Springer TA: Adhesion receptors of the immune system. *Nature* 346: 425–434, 1990
45. Daniel L, Sichez H, Giorgi R, Dussol B, Figarella-Branger D, Pellissier JF, Berland Y: Tubular lesions and tubular cell adhesion molecules for the prognosis of lupus nephritis. *Kidney Int* 60: 2215–2221, 2001
46. van Kooten C, Daha MR, van Es LA: Tubular epithelial cells: A critical cell type in the regulation of renal inflammatory processes. *Exp Nephrol* 7: 429–437, 1999
47. Remuzzi G, Ruggeneti P, Benigni A: Understanding the nature of renal disease progression. *Kidney Int* 51: 2–15, 1997
48. Furuta T, Saito T, Ootaka T, Soma J, Obara K, Keishi A, Yohinaga K: The role of macrophages in diabetic glomerulosclerosis. *Am J Kidney Dis* 21: 480–485, 1993